Crystal Structure of Murine 11β-Hydroxysteroid Dehydrogenase 1: An Important Therapeutic Target for Diabetes[‡]

Jiandong Zhang,[§] Timothy D. Osslund,[||] Matthew H. Plant,[⊥] Christi L. Clogston,[||] Rebecca E. Nybo,[⊥] Fei Xiong,[⊥] John M. Delaney,[⊥] and Steven R. Jordan*[,§]

Department of Molecular Structure, Amgen Inc., 1 Amgen Center Drive, Thousand Oaks, California 91320, Department of Pharmaceutics, Amgen Inc., 1 Amgen Center Drive, Thousand Oaks, California 91320, and Department of Protein Science, Amgen Inc., 1 Amgen Center Drive, Thousand Oaks, California 91320

Received November 12, 2004; Revised Manuscript Received March 10, 2005

ABSTRACT: 11β-Hydroxysteroid dehydrogenase type 1 (11β-HSD1) catalyzes the conversion of 11-dehydrocorticosterone to its active form corticosterone in rodents (or cortisone to cortisol in humans). The reductive reaction of the 11-keto to 11-hydroxyl is the pivotal switch in the activation of glucocorticoids. An excess of active glucocorticoids has been shown to play a key role in metabolic disorders such as diabetes and obesity. Therefore, 11β-HSD1 represents an important therapeutic target for the treatment of these diseases. To facilitate the iterative design of inhibitors, we have crystallized and determined the three-dimensional structures of a binary complex of murine 11β-HSD1 with NADP(H) to a resolution of 2.3 Å and of a ternary complex with corticosterone and NADP(H) to a resolution of 3.0 Å by X-ray crystallography. The enzyme forms a homodimer in the crystal and has a fold similar to those of other members of the family of short chain steroid dehydrogenases/reductases (SDRs). The structure shows a novel folding feature at the C-terminus of the enzyme. The C-terminal helix insertions provide additional dimer contacts, exert an influence on the conformations of the substrate binding loops, and present hydrophobic regions for potential membrane attachment. The structure also reveals how 11β-HSD1 achieves its selectivity for its substrate.

Glucocorticoids play important roles in a variety of physiological and cellular processes, including the regulation of metabolic enzymes, inflammatory responses, and blood pressure (*1*−*3*). The active hydroxyl form of glucocorticoids binds to nuclear receptors and subsequently influences gene transcriptions. The two isoforms of 11β-HSDs catalyze the interconversion between the 11-keto forms and the active 11-hydroxyl forms of glucocorticoids (Figure 1). Type 1 acts as a reductase, whereas type 2 acts as a dehydrogenase. A level of cortisol regulation is achieved by the differential tissue distribution of the two isoforms. 11β-HSD1[1] is expressed predominantly in liver, adipose, and brain, and type 2 is expressed mostly in kidney.

A variety of diseases, including insulin resistance/type 2 diabetes, dyslipidemia, and obesity, are induced by glucocorticoid excess. The therapeutic potential of 11β-HSD1 inhibition has been demonstrated by gene knockout and transgenic mouse models (*4*). Specifically, 11β-HSD1 null mice were found to resist high-fat diet-induced obesity. An improved lipid and lipoprotein profile, hepatic insulin sensitivity, and glucose tolerance have also been reported for the 11β-HSD1 gene knockout mice (*5*). The phenotype of transgenic mice overexpressing 11β-HSD1 selectively in adipose tissue has shown marked insulin resistance and hyperlipidemia (*4*). Further studies of these transgenics also linked overexpression of 11β-HSD1 to hypertension (*6*). 11β-HSD1 inhibitors have been synthesized and shown to be able to lower the expression levels of gluconeogenic enzymes and blood glucose and thus provide some degree of validation for the therapeutic potential of this class of inhibitors (*7*). Improving the potency and pharamaceutical properties of 11β-HSD1 inhibitors will be critical for the successful discovery of effective human therapeutic agents.

11β-HSD1 belongs to the SDR family of enzymes and uses NADPH as a cofactor. This family is characterized by a consensus GXXXGXG nucleotide binding motif and a conserved S-Y-K catalytic triad. Only the tyrosine residue is completely invariant. While most SDRs are soluble enzymes, 11β-HSD1 is linked to the endoplasmic reticulum (ER) membrane by an N-terminal single transmembrane segment with the catalytic domain localized in the lumen of the ER (*8*, *9*). Although native 11β-HSD1 is glycosylated, the unglycosylated enzyme is fully active (*10*).

11β-HSD1 possesses some unusual enzymatic properties. Although it acts as a reductase in vivo, it is bidirectional in vitro. The unidirectional function in vivo is a consequence of the high local concentration of the NADPH cofactor regenerated by hexose-6-phosphate dehydrogenase (*11*). 11β-

[‡] The atomic coordinates and structure factors [PDB entries 1Y5R for the binary complex of murine 11β-HSD1 with NADP(H) and 1Y5Mfor the ternary complex of 11β-HSD1 with corticosterone and NADP(H)] have been deposited in the Protein Data Bank.

* To whom correspondence should be addressed. J.Z.: phone, (805) 447-6735; fax, (805) 499-7464; e-mail, zhang@amgen.com. S.R.J.: phone, (805) 447-7148; fax, (805) 499-7464; e-mail, sjordan@amgen.com.

[§] Department of Molecular Structure.

[||] Department of Pharmaceutics.

[⊥] Department of Protein Science.

[1] Abbreviations: 11β-HSD1, 11β-hydroxysteroid dehydrogenase type 1; SDR, short chain steroid dehydrogenase/reductase.

10.1021/bi047599q CCC: $30.25
Published on Web 04/16/2005

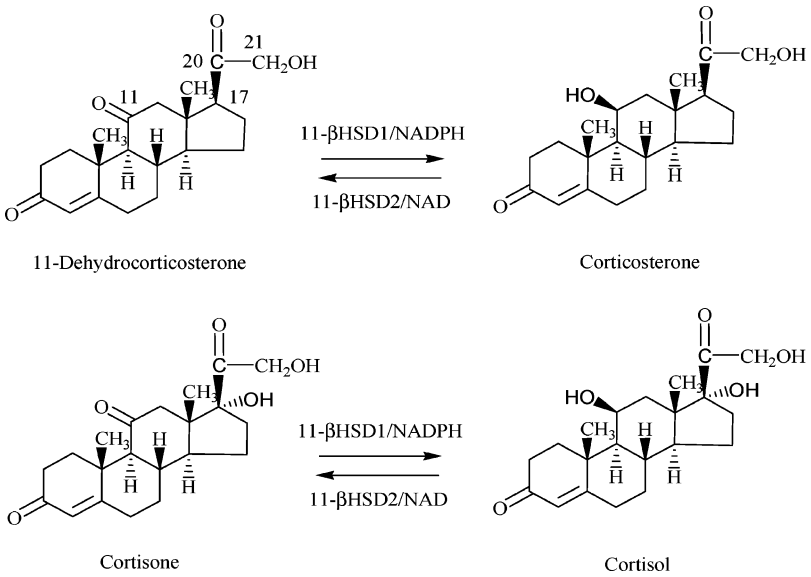

FIGURE 1: Reaction scheme in vivo. 11β-HSD1 acts as an oxoreductase converting dehydrocorticosterone to corticosterone in rodents and cortisone to cortisol in humans using NADPH as a cofactor. 11β-HSD2 acts as a dehydrogenase catalyzing the reverse reaction using NAD as a cofactor. Dehydrocorticosterone and cortisone are the inert forms of the hormone, whereas corticosterone and cortisol are the active forms of the hormone.

HSD1 has a low affinity for its substrate. The reported K_m of the enzyme, ranging from low micromolar to submicromolar values, is higher than the low nanomolar free-circulating substrate concentration (*12*, *13*). One explanation for this paradox is that the local concentration of the substrate is higher at the ER membrane. The biophysical characterization of the enzyme has yielded controversial results on the oligomerization state of the active enzyme due to the complications resulting from the presence of detergent for this membrane-associated protein. Both dimeric and tetrameric forms of the enzymes have been observed in solution (*12*, *14*).

Here we present the structures of the catalytic domain of murine 11β-HSD1 bound to NADP(H) in the presence and absence of the product corticosterone. The structure reveals a unique arrangement of the two C-terminal helices relative to other SDRs. These helices make additional cross-subunit interface contacts, and contribute to the conformations of the substrate binding segments. They also contain a cluster of hydrophobic residues on the protein surface that might be embedded in the membrane lipid bilayers. The atomic structure will aid in understanding the molecular basis for steroid recognition and in the structure-based drug design of potent and selective inhibitors of 11β-HSD1.

EXPERIMENTAL PROCEDURES

Expression and Purification. Murine 11β-HSD1 (residues 24−292) is expressed in *Escherichia coli* with a His_6 tag at the amino terminus. A PCR fragment comprising residues 24−292 (GENPEPT entry S75207) was amplified and subcloned into the NdeI−XhoI sites of a proprietary plasmid expression vector (*15*). PCR primers were designed to generate a gene fragment encoding residues 24−292 with addition of a 5′ NdeI site and a 3′ XhoI site. The 5′ primer also added coding sequence downstream of the NdeI site for the histidine tag. The amplified PCR product was digested with NdeI and XhoI and subcloned into the plasmid expression vector. Fermentation of *E. coli* containing the DNA sequence-confirmed plasmid was carried out at 37 °C during the initial growth phase and then shifted to 20 °C for chemical induction.

Cell paste was suspended in 20 mM Tris (pH 8.0), 150 mM NaCl, and 5 mM benzamidine. The cell suspension was broken with two passes through a microfluidizer, and mixed with a buffer containing 5% glycerol, 0.1% Triton X-100, and 5 mM imidazole. The mixture was loaded on a Ni−NTA column. The Ni−NTA eluate was concentrated and processed by size exclusion chromatography (Sephacryl S200, Pharmacia) in 20 mM Tris (pH 8.0), 200 mM NaCl, 0.1% Triton, 5% glycerol, and 2 mM EDTA. The pool from the S200 column was concentrated and frozen at −80 °C. A frozen sample was thawed and passed through a Pierce Extracti-Gel D column using the same buffer without the detergent at room temperature and concentrated to 25 mg/mL for crystallization experiments.

Crystallization and Data Collection. The enzyme was crystallized by the vapor diffusion method using hanging drops. The protein sample was mixed with an equal volume of well solution of 1.8 M Li_2SO_4 and 0.1 M HEPES buffer (pH 7.5) at room temperature. The crystals belong to space group $P4_122$ with two molecules in the asymmetric unit with the following cell dimensions: $a = b = 96.72$ Å and $c = 219.30$ Å. A heavy atom derivative of the crystal was obtained by adding 1 mM ethylmercuric chloride to the crystal drop. The ternary complex was obtained by soaking 0.05 mM corticosterone and 1 mM NADPH into the crystal. Data were collected at beamline 5.0.2 at the Advanced Light Source using an ADSCQ315 detector and processed using HKL2000 (*16*). The cell dimensions for the ternary complex are close to the native crystal: $a = b = 96.99$ Å and $c = 218.15$ Å. The data statistics are summarized in Table 1.

Structure Solution and Refinement. The phases were obtained by single isomorphous replacement with the anomalous signal method using SOLVE (*17*). The overall figure of merit (from 40 to 2.5 Å) was 0.3. The electron density map was further improved using DM in the CCP4

Table 1: Refinement Statistics for the Binary Complex, Hg Derivative, and Ternary Complex of 11β-HSD1

	binary complex	Hg derivative	ternary complex
R_{merge}[a] (%) (last shell)	7.4 (45)	8.9 (60)	6.1 (22.5)
d_{min}	2.3	2.3	3.0
no. of measurements	918692	515636	637975
no. of unique data	47146	47146	21295
no. of reflections ($F > 0$)	43963		21295
completeness (%)	93		98.3
total no. of atoms	4424		4276
R-factor[b] (%)	21.9		21.0
R_{free}[c] (%)	25.0		24.7
no. of water molecules	148		0
no. of sulfate ions	4		0
no. of octane molecules	2		0
no. of corticosterones	0		2
no. of NADPHs	2		2
rms deviation			
bond lengths (Å)	0.0828		0.119
bond angles (deg)	1.786		1.763
Ramachandran regions[d] (%)			
residues in most favored regions	90		87.7
residues in additional allowed regions	9.7		11.4
residues in generously allowed regions	0.2		0.8

[a] $R_{merge} = \sum|I_i - \langle I\rangle|/\sum I_i$, where I_i is the intensity of an individual measurement and $\langle I\rangle$ is the mean intensity of this measurement. [b] R-factor $= \sum||F_{obs}| - |F_{calc}||/\sum|F_{obs}|$, where F_{obs} and F_{calc} are the observed and calculated structure factor amplitudes, respectively. [c] R_{free} was calculated using a subset (8%) of randomly chosen data that was excluded from refinement. [d] As calculated using PROCHECK in the CCP4 suite (*18*).

suite (*18*). The final figure of merit was 0.75 after solvent flattening by DM. The model was built using QUANTA (Accelrys). The model was refined using CNX (*19*), and the refinement statistics are summarized in Table 1.

RESULTS

Overall Fold of the Subunits. The final model contains two monomers that form a homodimer. There is clear electron density for residues 25−289 for each monomer. Representative electron density maps are shown in Figure 2 with the atoms labeled for the two different structure solutions. The Cα trace of one monomer is shown in Figure 3. The overall fold is similar to those of other SDR family members (*20*). The consensus fold consists of the central seven-stranded parallel β-sheet, flanked by six parallel α-helices (Figure 3). There are four short α-helix insertions relative to the consensus fold (Figure 4): αEF (residues 171−174) between αE and αF, αFG (residues 220−228) between βF and αG, and two sequential helices (αH1 and αH2) following βG. The αFG insertion is also part of the substrate entry loop (residues 216−231). Helices αH1 and αH2 are located at the C-terminus of the enzyme. The pseudo-2-fold axis places the amino termini on the same face of the dimer so that the amino-terminal residues for each chain point in the same direction toward the membrane. The orientation of the N-termini makes it possible for the cluster of the solvent-exposed hydrophobic residues on C-terminal helices αH1 and αH2 to become embedded in the membrane. Contrary to previous studies (*8*), none of the cysteine residues form disulfide bonds. The closest approach of the cysteines is made by C213 and C241, but the sulfur atoms are more than 8 Å apart.

Subunit Interface. The enzyme was crystallized with a dimer in the asymmetric unit. The structures of the two

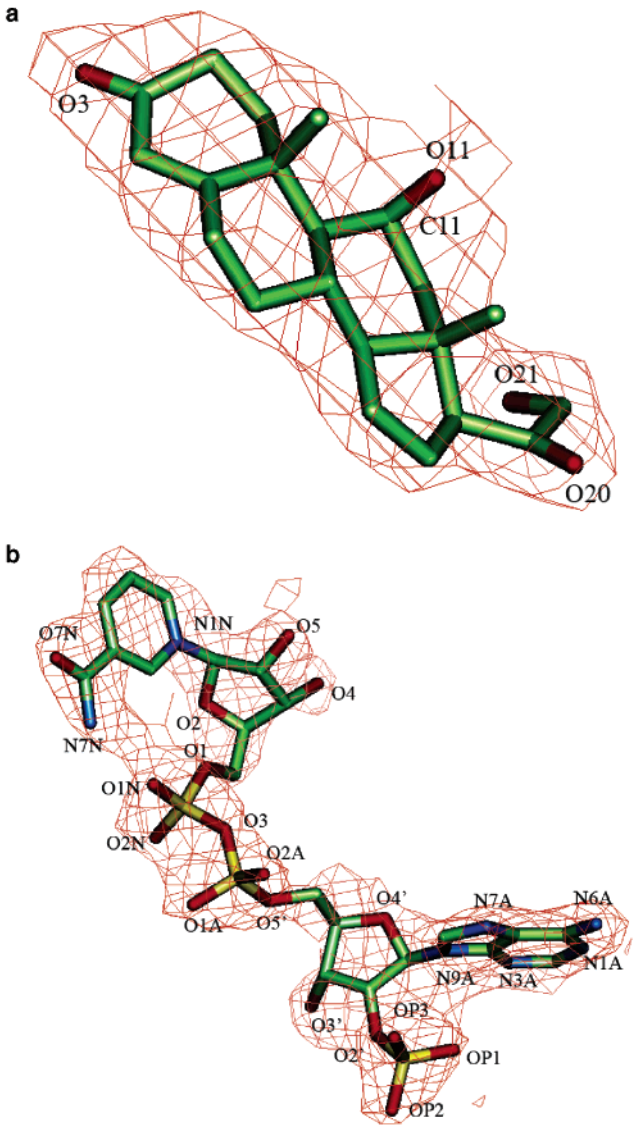

FIGURE 2: Electron density map contoured at 1σ for corticosterone (a) in the ternary complex and NADPH (b) in the binary enzyme. The map was calculated using the $2|F_o| - |F_c|$ coefficients and final model-derived phases.

subunits superimpose well on each other with an rms deviation of 0.24 Å for the backbone atoms in the NADP(H) complex and an rms deviation of 0.31 Å for the ternary complex. The two subunits are related by a pseudo-2-fold axis, designated as the *Q*-axis using the convention described by Ghosh (*21*) (Figure 5). The total buried surface area of the dimer interface is large, ~5129 Å^2.

Although αH1 and αH2 do not make direct contacts with the substrate, they make intimate interactions with two of the substrate binding loops in the other subunit. This is in contrast to the 7α-HSD structure in which the C-terminus wraps back on the same subunit and forms part of the substrate-binding site (*22*). Helices αH1 and αH2 in 11β-HSD1 may support the substrate binding loops to adopt the proper conformations to accommodate the substrate. The segment of residues 273−284 (αH2) interacts with the αEF−αF turn (residues 174−178) in the substrate binding loop (residues 170−183) as described below. The segment of residues 283−288 (αH2) makes contacts with residues 231−233 (αFG−αG loop), the C-terminal residues of the substrate

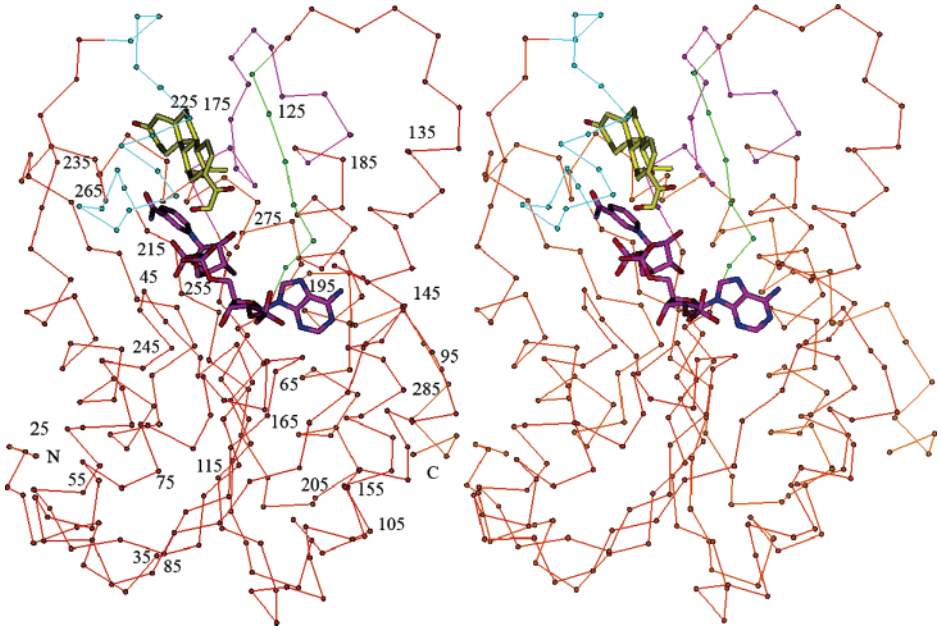

FIGURE 3: Stereoview of the 11β-HSD1 monomer Cα trace drawn by InsightII (Accelyrs Inc.). The corticosterone and cofactor NADPH are respresented with a stick model. Residues are numbered every 10 residues. Substrate-binding segments are colored differently, with residues 121−126 in green, residues 170−183 in purple, and residues 216−231 in cyan.

entry loop (residues 216−231). The only major interactions of helices αH1 and αH2 with the same subunit are between two nitrogens of the guanidinium group of R273 in αH2 and the two carboxylate oxygens of D191 in αF. C-Terminal cross-subunit contacts have also been observed for two other SDRs, 17β-HSD (*23*) and (3*R*)-hydroxyacyl-CoA dehydrogease (*25*).

As in the *Q*-axis interfaces in other SDRs, the 11β-HSD1 dimer interface also consists of a four-helix bundle of αE and αF from each monomer. In addition to the helix−helix interactions, helix−loop packing also occurs at the interface. Four segments are involved in the intermolecular contacts: 127−152 (βD−αE turn and αE), 174−204 (αEF−αF turn and αF), 229−233 (αFG−αG turn), and 267−288 (αH1 and αH2) (Figure 5). The βD−αE turn (F129) packs against αF; the αEF−αF turn (residues 174−178) packs against αH2, and the αEF−αF turn (residues 176−179) packs against αF.

Cofactor NADP(H) Binding Site. In the crystals grown without the addition of corticosterone, an NADP(H) molecule was bound in the enzyme (Figure 2b), even though no additional NADP(H) was added during the protein purification or crystallization process. The conformation and orientation of NADP(H) are very similar to those found in other SDRs, shown in Figure 3. It sits in a cleft formed by seven segments of the enzyme: residues 41−46, 65 and 66, 91−93, 119−121, 168 and 169, 183−187, and 215−222 (Figure 3 and Table 2).

The NADP(H) makes extensive polar and charged interactions with the enzyme, as shown in Table 2 and Figure 6. The hydrophobic interactions are mostly through the nicotinamide and adenine portions of the cofactor. The nicotinamide makes contacts with the corticosterone and the side chain of L215. The orientations of the nicotinamide and adenine are also stabilized through polar or charged interactions as shown in Table 2. The side chain R66 neutralizes the negative charge of the 2′-phosphate of NADP(H) and makes hydrophobic stacking interactions with the adenine of NADP(H). However, in human 17β-HSD (*26*), the 2′-phosphate neutralizing arginine residue at the equivalent position does not have the stacking interaction with the adenine group. In the trihydroxynaphthalene reductase structure, R39 that comes from a different structural element interacts with the 2′-phosphate of NADPH (*27*). While it appears that a neutralizing arginine residue interacting with the 2′-phosphate of NADPH is required to distinguish whether an SDR will use NADPH or NADH as a cofactor, the arginine residue can occur at different locations in the primary sequence.

The backbone atoms of the ^{215}LGLI^{218} loop in 11β-HSD1 form four hydrogen bonds with the nicotinamide of the cofactor: L215 O and C5N (3.4 Å), G216 O and C4N (3.0 Å), I218 N and O7N (2.7 Å), and I218 O and N7N (3.3 Å). Hydride transfer occurs on C4 of nicotinamide in the *pro-S* configuration during catalysis. Therefore, the conserved interaction of the backbone carbonyl group of G216 with the *pro-R* hydrogen of C4 of the nicotinamide has been suggested to be important for catalysis (*28*). The Pro-Gly sequence, equivalent to L215 and G216 of 11β-HSD1, is preferred for SDR enzymes. Although this sequence has variations, the three hydrogen bonds between C4N, O7N, and N7N of the nicotinamide and the enzyme backbone atoms have been observed in all the known SDR structures. The backbone carbonyl group of L215 also forms a hydrogen bond with the L171 backbone nitrogen atom. Most of the SDR enzymes also have similar hydrogen bonds such as L215 in 11β-HSD1: the carbonyl group of L215 with the backbone nitrogen atom of the residue after the catalytic serine and with C5 of nicotinamide. However, L215 interactions do not appear to be essential for catalysis, because in the structure of the rat (3*R*)-hydroxyacyl-CoA dehydrogenase, equivalent interactions of L215 are absent (*25*).

The catalytic residue K187 makes bifurcated hydrogen bonds with O4 and O5 of the nicotinamide ribose, whereas the OH group of catalytic residue Y183 is hydrogen bonded with O5 of the same ribose. Similar interactions have been observed in most known SDR structures. This is consistent

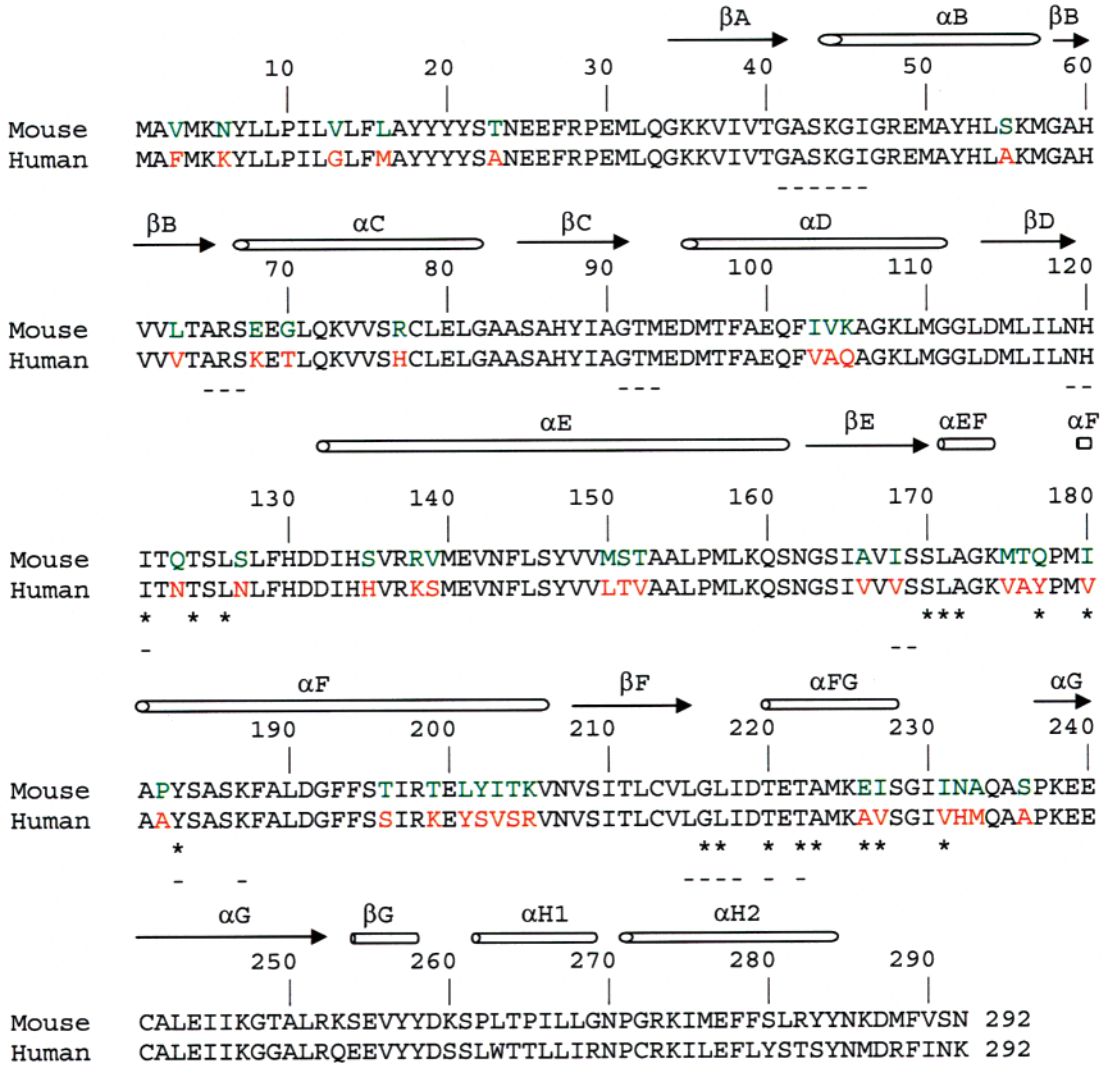

FIGURE 4: Sequence alignment of murine and human 11β-HSD1. Arrows or cylinders above the sequence indicate secondary structures. Residues contacting the steroid are denoted with an asterisk, whereas residues contacting NADPH are denoted with a dash; 81% of the residues are identical.

with the catalytic mechanism in which K187 maintains the orientation of the nicotinamide ribose and aids in deprotonation of the hydroxyl of Y183 (*22*).

Substrate-Binding Site. For both structures determined in the presence and absence of corticosterone, there is strong electron density in the substrate-binding site (Figure 2a). In the structure grown in the absence of substrate, a detergent molecule is observed and was modeled as an eight-carbon chain bound in the steroid-binding site with an extended conformation leading toward the bulk solvent. For the crystals soaked with corticosterone, the molecule is clearly visible in the difference density maps. We presume that it is still in the reduced state because excess NADPH (1 mM) was added with corticosterone (0.05 mM) to form the ternary complex. The resolution of these structures is not sufficient to determine the oxidation state of the reactants. They can be modeled into the electron density equally well in either oxidation state. The lack of a structural preference for the substrate or product is consistent with the reversibility of the enzyme.

In the corticosterone complex structure, the corticosterone is positioned between three substrate-binding segments of the protein: residues 121−126 (βD−αE turn), 170−183 (αEG, αEF−αF turn, and αF), and 216−231 (βF−αFG turn, αFG, and αFG−αG turn). The detailed interactions are shown in Figure 6. The corticosterone is mostly buried with only 13% of its surface accessible to the solvent. The polar oxygens at opposite sides of the substrate are open to solvent by two different channels. The possible hydrogen bonds are listed in Table 2. The α-side of the corticosterone interacts with residues G216, L217, T220, T222, A223, E226, I227, and I231 of the substrate entry loop of residues 216−231, and the nicotinamide from the cofactor. The total buried surface area between the substrate and NADP(H) is ~65 Å^2. The α-side of corticosterone makes contacts with I121, T124, and L126 from the binding loop of residues 121−126 and S170, L171, A172, Q177, I180, and Y183 from the binding loop of residues 170−183. The hydroxyl groups of catalytic residues S170 and Y183 interact directly with the O11 atom of corticosterone.

O21 and O20 hold a trans conformation in the refined model. This orientation was the best fit to the original electron density maps and maintained that orientation throughout subsequent refinement. It should be noted that the trans conformation in steroids has not been observed before. Considering the medium resolution of the X-ray data,

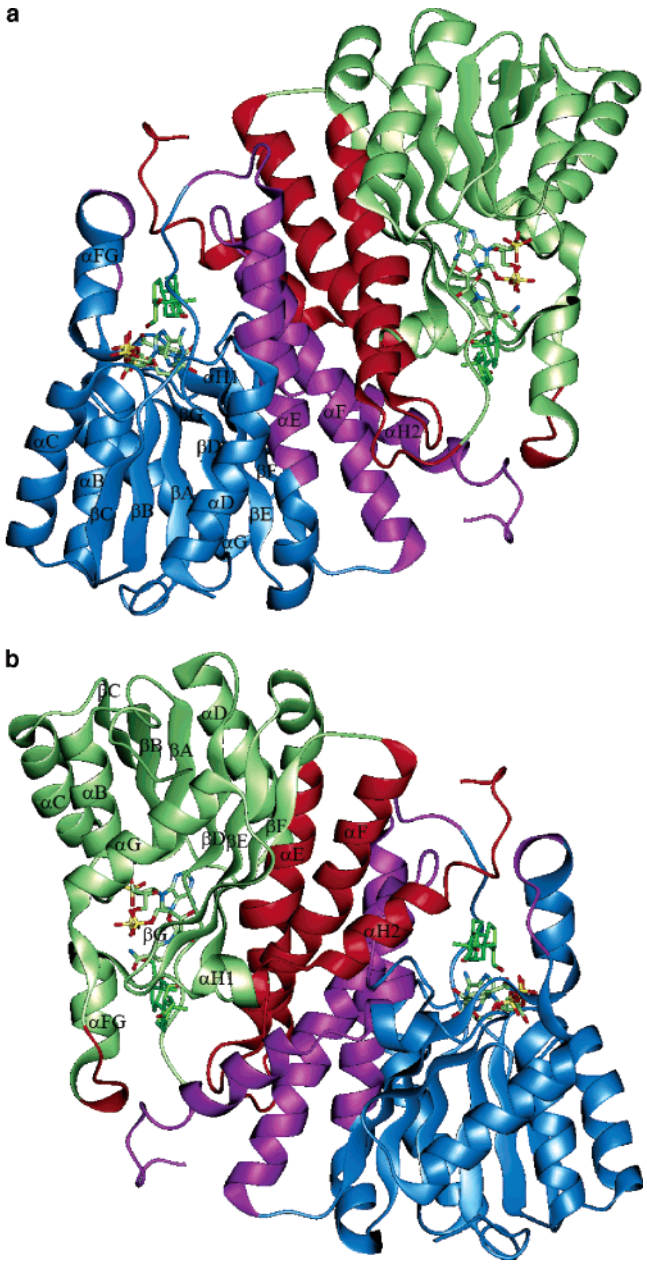

FIGURE 5: (a) Ribbon diagram of the 11β-HSD1 dimer. Subunit A is colored blue, and subunit B is colored green. Segments of residues 127−152, 174−204, 229−233, and 267−288 at the interface of the dimer are colored purple in subunit A and red in subunit B. A stick drawing of corticosterone and NADPH is also shown. (b) Different orientation of panel a with a 180° rotation of the *Y*-axis. In both panels a and b, the two subunits are related by the *Q*-axis perpendicular to the paper.

3.0 Å, we cannot rule out the possibility that O21 may hold an energetically more favorable cis conformation with respect to O20. The energy loss due to the missing intramolecular hydrogen bond of O21 and O20 in the trans conformation may be compensated by favorable interactions with the cofactor. O21 acts as both a hydrogen bond acceptor from N7N of the nicotinamide and a hydrogen bond donor to the O1N atom of the NADPH.

Although SDRs share a similar fold, their substrate-binding loops and the C-terminus of the enzyme have shown the most divergent conformations. Consequently, the overall shape, solvent accessible regions, and polar composition of the steroid-binding groove are very different among SDR members. While the pocket is composed of mostly hydrophobic residues, the hydroxyl groups of Y183 and S170 and the backbone nitrogen atoms of L171 and A172 provide potential polar interactions with inhibitors. The two solvent channels on either end of the steroid-binding site provide regions where inhibitor design efforts may be exploited.

Table 2: Polar Interactions between Corticosterone, NADPH, and 11β-HSD1 (subunit A) in the Ternary Complex

atom in corticosterone	atom in 11β-HSD1 and NADPH	distance (Å)
O3	Q177 N2	4.5
O3	L217 N	3.9
O11	S170 O	3.1
O11	Y183 OH	2.8
O20	T124 N	4.5
O21	T222 O	3.6
O21	NADP(H) O1N	2.9
O21	NADP(H) N7N	3.4

atom in NADPH	atom in 11β-HSD1 and corticosterone	distance (Å)
O7N	I218 N	2.7
C4N	G216 O	3.0
C5N	L215 O	3.4
N7N	I218 O	3.3
N7N	T220 O	3.3
N7N	corticosterone O4	3.4
N7N	NADP(H) O1N	3.0
O4	K187 NZ	3.2
O4	N119 O	2.7
O5	K187 NZ	3.2
O5	Y183 OH	2.7
O2N	I46 N	2.9
O2A	T222 O	3.0
O1A	T222 O	3.7
O1A	G45 N	4.0
O1A	K44 NZ	4.0
O3′	K44 N	3.3
O3′	S43 O	3.7
O4′	I121 N	3.8
N1A	M93 N	2.8
N6A	T92 O	3.3
O2	S43 O	3.8
OP1	R66 N	3.0
OP1	R66 N	2.7
OP2	S67 N	3.3
OP2	S43 O	3.5
OP3	R66 NH2	2.9

The αEF α-turn (residues 171−174) immediately following the catalytic residue S170 exists in all known SDR structures that contain a catalytic serine residue. It was first described in the structure of rat (3*R*)-hydroxyacyl-CoA dehydrogease (*29*). The SDRs that do not contain the catalytic serine residues, e.g., enonyl-ACP reductase (*30*), also lack the αEF α-turn. In the 11β-HSD1−corticosterone structure, the hydroxyl group of S170 forms two possible hydrogen bonds with two backbone nitrogen atoms, L171 N (∼2.7 Å) and A172 N (∼3.2 Å) in αEF. These two backbone amide groups serve as hydrogen bond donors to the S170 hydroxyl group and position the proton of the OH group of S170 close to the 11β-oxygen of the corticosterone. This important proton network suggests that the αEF turn plays an essential role in catalysis. This is consistent with the structural conservation of αEF among the SDRs with an S-Y-K catalytic triad.

The residues of the steroid-binding sites show minimal movement upon binding of substrate. The only significant

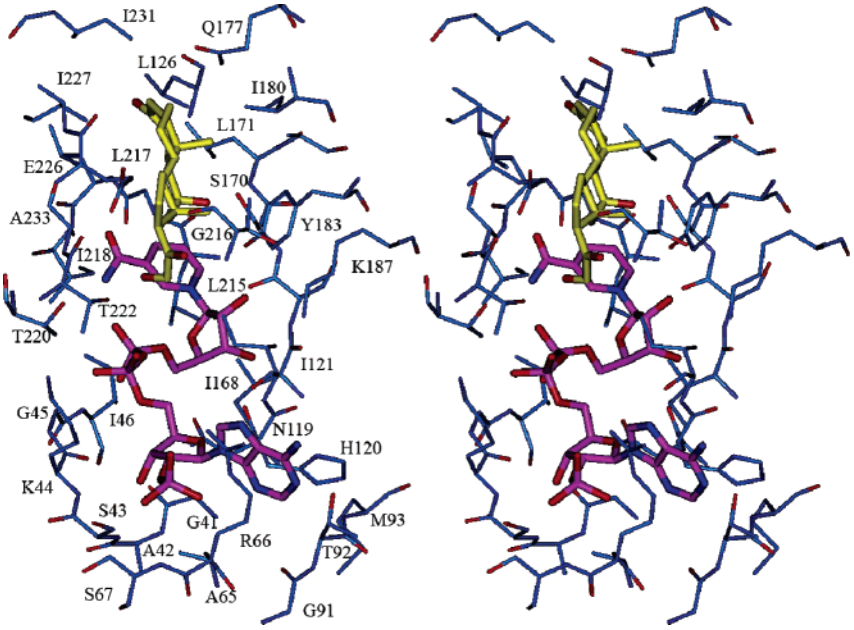

FIGURE 6: Stereoview of 11β-HSD1 binding sites of corticosterone and cofactor NADPH. C atoms of corticosterone, NADPH, and the enzyme are colored yellow, purple, and blue, respectively. O atoms are colored red, and N atoms are colored blue. Figures were produced in InsightII (Accelyrs Inc.).

conformational change is that the hydroxyl group of S170 turns 90° toward the corticosterone and forms a hydrogen bond. It forms four possible polar interactions with L171 N (~3.4 Å), A172 N (~3.4 Å), G173 N (4.0 Å), and Y183 OH (~3.1 Å) in the absence of the substrate. It might be possible that after catalysis occurs, a hydrogen bond also forms between the OH groups of catalytic residues S170 and Y183 so that the interactions between the enzyme and product are weakened to facilitate the process of the product leaving the active site.

In the SRD enzyme family, the segment containing residues 216−231 is called the substrate entry loop because it often adopts different conformations in structures with and without substrate. In the 11β-HSD1 structures reported here, the substrate entry loop does not change conformations when the reaction product is soaked in. One reason might be that the detergent molecule in the substrate site holds the substrate entry loop close to the steroid-bound conformation. Alternatively, it might be that the crystal lattice prevents dramatic conformational changes since the structure is obtained by soaking in the product. The rms deviation of structures with or without corticosterone is only 0.12 Å. For many other SDR family members, two proline residues are postulated as the hinges for the movement of the substrate entry loop as in *E. coli* 7α-HSD (*22*). However, in 11β-HSD1, there are no corresponding prolines.

Comparison of the Murine and Human Structures. The murine and human enzymes share virtually identical folds and dimeric organization (Figure 7a). The rms deviation of the Cα atoms of the murine and the human dimers (molecules A and B from PDB entry 1XU7) is only 0.46 Å. The two subunits of the murine dimer are more similar, with a Cα rms deviation of only 0.13 Å, whereas the Cα rms deviation of the two subunits of the human dimer is 0.42 Å. The larger difference results from the different conformations of the segment of residues 228−233 in the human enzyme. The segment of residues 228−233 in the mouse enzyme is aligned well with molecule B of the human enzyme and takes different conformations with molecule A of the human enzyme. This segment is part of the substrate entry loop and has been observed to be the most flexible in most SDRs. The corresponding residues surrounding NAPDH in the human enzyme are almost identical to those in the murine enzyme with only one conservative substitution at position 168: an isoleucine residue in mouse and a valine residue in human (Figure 7b).

Although the natural substrates for human and murine 11β-HSD1 are different by an additional hydroxyl group in the C17α position, the active site residues are mostly conserved. There are five amino acid substitutions (Figures 4 and 7b) with most of them being conservative substitutions: isoleucines at positions 180, 277, and 231 in the murine enzyme and valines in the human enzyme. The substitution closest to the C17 position of the substrate is residue 226. The side chain of E226 in the human enzyme points toward the solvent, and the Cβ atom is aligned well with the Cβ atom of A226 in the mouse enzyme. The largest difference is Q177 in mouse, and Y177 in human enzyme, but this residue is not near the C17 position. Despite the fact that the different species utilize slightly different forms of the steroid, there are comparable kinetics for the human enzyme using the mouse substrate and the mouse enzyme will recognize the human substrate. The K_m for cortisone in the mouse enzyme is 842.6 ± 130.8 nM, and the K_m for the human enzyme is 696.6 ± 339.5 nM (unpublished data). The slight difference in the K_m of cortisone is consistent with the small changes in the substrate-binding site residues. There are no obvious clashes when the human substrate is modeled into the mouse active site; therefore, the murine 11β-HSD1 structure is a reliable model for the design of inhibitors of the human enzyme. Most of the conserved residues have similar orientations between the murine and human enzymes with only one exception for S170 (Figure 7b), which has been shown to be able to take different conformations in the murine enzyme upon substrate binding.

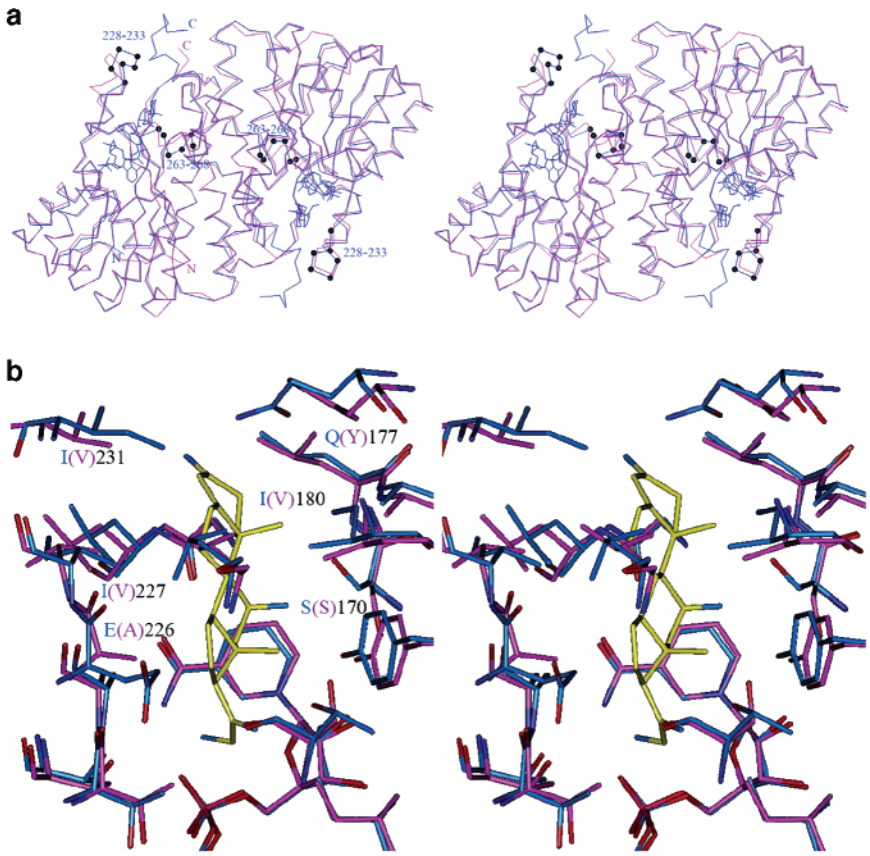

FIGURE 7: (a) Stereoview of the superimposition of Cα atoms of the murine and human 11β-HSD1. The Cα atoms of the murine and human enzymes are colored blue and purple, respectively. NADPH and corticosterone in the murine complex are colored blue. The two segments that have a more pronounced structural difference, residues 228−233 and 263−268, are labeled. The Cα atoms in these segments of the murine enzyme are represented by spheres. (b) Stereoview of the steroid-binding site of the superimposed murine and human structures. Carbon atoms of the murine are colored blue and the human atoms purple. The steroid carbon atoms from the murine structure are colored yellow. The five nonconserved active site residues are indicated with the human residue in parentheses. The conserved serine 170 position is shown for the murine structure as complexed with the steroid. The conformation of the human serine 170 occupies a similar position as the murine binary structure in the absence of the steroid.

DISCUSSION

The structures of the murine 11β-HSD1 complexes reported here provide a detailed analysis of the substrate recognition and structural elements for catalysis. 11β-HSD1 has been widely recognized as a potential therapeutic target for treatment of a variety of diseases such as diabetes type II, obesity, hyperglycemia, and hypertension. The distinctive steroid-binding site revealed by the structure makes the enzyme an ideal target for structure-based inhibitor design.

The arrangement of the C-terminal helix insertions, αH1 and αH2, is unique compared with the arrangements of other SDR family members. They play multiple roles in maintaining the enzyme structure. They form an extensive dimer interface, and interact with the substrate-binding loops. More importantly, they present a large continuous hydrophobic region on the protein surface for potential interactions with the membrane lipid bilayer.

The recently reported human 11β-HSD1 structure shows virtually the same fold as the mouse enzyme in both monomeric and dimeric forms (*14*). A tetramer of the enzyme of the human enzyme was found in one crystallographic asymmetric unit and was proposed to be the functional unit in vivo. In the murine enzyme, a crystallographic 2-fold axis perpendicular to the pseudo-2-fold axis of the dimer gives rise to a similar tetrameric organization. C-terminal helices αH1 and αH2 from each monomer form a pseudo-four-helix bundle in this interface. Consequently, the hydrophobic region on the protein surface from the C-terminal helix insertions becomes buried in this interface.

Membrane-associated proteins are known to aggregate in solutions, so the observed dimer−dimer formation of the murine enzyme in the crystal lattice may be an artifact in vitro. The total buried area in the *Q*-axis dimer interface, ∼5129 Å^2, is consistent with other known interfaces; however, the buried area of the dimer−dimer interface is only ∼618 Å^2 which is comparable to that formed by crystal lattice contacts. In a study of protein interactions, the smallest observed protein dimer interface was ∼1150 Å^2 (*31*). Given the very small contact area in the dimer−dimer interface, it is likely that the enzyme exists as a dimer with C-terminal helices buried in the membrane lipid bilayer while the enzyme is linked to the ER membrane. The proximity of the enzyme to the membrane suggests that a potentially higher substrate concentration in the ER membrane by metabolism can drive the catalysis even though the enzyme has low affinity for its substrate.

Interestingly, the C-terminal helix insertions that make extra dimer contacts result in an unusually large interface, ∼5129 Å^2, 18.8% of the molecular surface. The "large" contact area in protein dimers ranges from 2000 to 4600 Å^2 according to a study of protein structures dated to 1998 (*31*).

The large contact area might be needed as a fail-safe mechanism to ensure that dimer formation is not disrupted by the presence of a nearby membrane lipid.

The short αEF α-helix following the catalytic serine residue is a conserved structural element for SDRs containing the S-Y-K catalytic triad. We propose that the αEF helix may play a crucial role in positioning the hydroxyl group of catalytic residue S170 and thus be essential for catalysis. It will be interesting to see whether future SDR structures maintain the correlation between the presence of an αEF segment and the catalytic serine in the S-Y-K triad.

Despite the fact that the natural ligands for mouse and human 11β-HSD1 are different, the murine structure will provide a reliable model for the design of inhibitors for the human enzyme. There are relatively few amino acid changes in the active site. Moreover, we have identified a number of inhibitors that do cross react (unpublished data). Selectivity between 11β-HSD1 and 11β-HSD2 is also essential for human therapeutic use because they are antagonistic to each other in vivo. Although some inhibitors such as glycyrrhetinic acid and carbenoxolone can inhibit both enzymes, most of the reported 11β-HSD1 inhibitors are selective for type 1 over type 2 (*32*, *33*). This is expected because there is only 15% sequence identity between 11β-HSD1 and 11β-HSD2. This set of structure determinations provides significant aid in the design of potent and selective inhibitors of 11β-HSD1 for the treatment of a number of human diseases. We have developed a system in which the detergent molecule can be replaced by a ligand in the crystal, so it is now possible to soak in novel inhibitors for an efficient iterative rational drug design process.

ACKNOWLEDGMENT

We thank Clarence Hale, Minghan Wang, Rashid Syed, Michael Bartberger, Richard Lindberg, and Elizabeth Goldsmith for helpful discussion and reading the manuscript. We also thank the Advanced Light Source staff at beamline 5.0.2 for their support. The Advanced Light Source is supported by the Director, Office of Science, Office of Basic Energy Sciences, Materials Sciences Division, of the U.S. Department of Energy under Contract DE-AC03-76SF00098 at Lawrence Berkeley National Laboratory.

REFERENCES

1. Stewart, P. M., and Krozowski, Z. S. (1999) 11-Hydroxysteroid dehydrogenase, *Vitam. Horm. 57*, 249−324.
2. Kotelevtsev, Y., Holmes, M. C., Burchell, A., Houston, P. M., Schmoll, D., Jamieson, P., Best, R., Brown, R., Edwards, C. R., Seckl, J. R., and Mullins, J. J. (1997) 11β-Hydroxysteroid dehydrogenase type 1 knockout mice show attenuated glucocorticoid-inducible responses and resist hyperglycemia on obesity or stress, *Proc. Natl. Acad. Sci. U.S.A. 94*, 14924−14929.
3. Tomlinson, J. W., and Stewart, P. M. (2001) Cortisol metabolism and the role of 11β-hydroxysteroid dehydrogenase, *Best Pract. Res., Clin. Endocrinol. Metab. 15*, 61−78.
4. Masuzaki, H., Paterson, J., Shinyama, H., Morton, N. M., Mullins, J. J., Seckl, J. R., and Flier, J. S. (2001) A transgenic model of visceral obesity and the metabolic syndrome, *Science 294*, 2166−2170.
5. Morton, N. M., Holmes, M. C., Fievet, C., Staels, B., Tailleux, A., Mullins, J. J., and Seckl, J. R. (2001) Improved lipid and lipoprotein profile, hepatic insulin sensitivity, and glucose tolerance in 11β-hydroxysteroid dehydrogenase type 1 null mice, *J. Biol. Chem. 276*, 41293−41300.
6. Masuzaki, H., Yamamoto, H., Kenyon, C. J., Elmquist, J. K., Morton, N. M., Paterson, J. M., Shinyama, H., Sharp, M. G., Fleming, S., Mullins, J. J., Seckl, J. R., and Flier, J. S. (2003) Transgenic amplification of glucocorticoid action in adipose tissue causes high blood pressure in mice, *J. Clin. Invest. 112*, 83−90.
7. Alberts, P., Engblom, L., Edling, N., Forsgren, M., Klingstrom, G., Larsson, C., Ronquist-Nii, Y., Ohman, B., and Abrahmsen, L. (2002) Selective inhibition of 11β-hydroxysteroid dehydrogenase type 1 decreases blood glucose concentrations in hyperglycaemic mice, *Diabetologia 45*, 1528−1532.
8. Ozols, J. (1995) Lumenal orientation and post-translational modifications of the liver microsomal 11β-hydroxysteroid dehydrogenase, *J. Biol. Chem. 270*, 2305−2312.
9. Odermatt, A., Arnold, P., Stauffer, A., Frey, B. M., and Frey, F. J. (1999) The N-terminal anchor sequences of 11β-hydroxysteroid dehydrogenases determine their orientation in the endoplasmic reticulum membrane, *J. Biol. Chem. 274*, 28762−28770.
10. Blum, A., Martin, H. J., and Maser, E. (2000) Human 11β-hydroxysteroid dehydrogenase type 1 is enzymatically active in its nonglycosylated form, *Biochem. Biophys. Res. Commun. 276*, 428−434.
11. Atanasov, A. G., Nashev, L. G., Schweizer, R. A., Frick, C., and Odermatt, A. (2004) Hexose-6-phosphate dehydrogenase determines the reaction direction of 11β-hydroxysteroid dehydrogenase type 1 as an oxoreductase, *FEBS Lett. 571*, 129−133.
12. Maser, E., Volker, B., and Friebertshauser, J. (2002) 11β-Hydroxysteroid dehydrogenase type 1 from human liver: Dimerization and enzyme cooperativity support its postulated role as glucocorticoid reductase, *Biochemistry 41*, 2459−2465.
13. Frick, C., Atanasov, A. G., Arnold, P., Ozols, J., and Odermatt, A. (2004) Appropriate function of 11β-hydroxysteroid dehydrogenase type 1 in the endoplasmic reticulum lumen is dependent on its N-terminal region sharing similar topological determinants with 50-kDa esterase, *J. Biol. Chem. 279*, 31131−31138.
14. Hosfield, D. J., Wu, Y., Skene, R. J., Hilger, M., Jennings, A., Snell, G. P., and Aertgeerts, K. (2004) Conformational Flexibility in Crystal Structures of Human 11β-HSD1 Provide Insights into Glucocorticoid Interconversion and Enzyme Regulation, *J. Biol. Chem.* (in press).
15. Lacey, D. L., Timms, E., Tan, H. L., Kelley, M. J., Dunstan, C. R., Burgess, T., Elliott, R., Colombero, A., Elliott, G., Scully, S., Hsu, H., Sullivan, J., Hawkins, N., Davy, E., Capparelli, C., Eli, A., Qian, Y. X., Kaufman, S., Sarosi, I., Shalhoub, V., Senaldi, G., Guo, J., Delaney, J., and Boyle, W. J. (1998) Osteoprotegerin ligand is a cytokine that regulates osteoclast differentiation and activation, *Cell 93*, 165−176.
16. Otwinowski, Z., and Minor, W. (1997) Processing of X-ray Diffraction Data Collected in Oscillation Mode, *Methods Enzymol. 276*, 307−326.
17. Terwilliger, T. C., and Berendzen, J. (1999) Automated MAD and MIR structure solution, *Acta Crystallogr. D55*, 849−861.
18. Bailey, S. (1994) The ccp4 suite: Programs for protein crystallography, *Acta Crystallogr. D50*, 760−763.
19. Brunger, A. T., Adams, P. D., Clore, G. M., Delano, W. L., Gros, P., Grossekunstleve, R. W., Jiang, J. S., Kuszewski, J., Nilges, M., Pannu, N. S., Read, R. J., Rice, L. M., Simonson, T., and Warren, G. L. (1998) Crystallography and NMR system: A new software suite for macromolecular structure determination, *Acta Crystallogr. D54*, 905−921.
20. Lesk, A. M. (1995) NAD-binding domains of dehydrogenases, *Curr. Opin. Struct. Biol. 5*, 775−783.
21. Ghosh, D., Weeks, C. M., Grochulski, P., Duax, W. L., Erman, M., Rimsay, R. L., and Orr, J. C. (1991) Three-dimensional structure of holo 3,20β-hydroxysteroid dehydrogenase: A member of a short-chain dehydrogenase family, *Proc. Natl. Acad. Sci. U.S.A. 88*, 10064−10068.
22. Tanaka, N., Nonaka, T., Tanabe, T., Yoshimoto, T., Tsuru, D., and Mitsui, Y. (1996) Crystal structures of the binary and ternary complexes of 7β-hydroxysteroid dehydrogenase from *Escherichia coli*, *Biochemistry 35*, 7715−7730.
23. Sawicki, M. W., Erman, M., Puranen, T., Vihko, P., and Ghosh, D. (1999) Structure of the ternary complex of human 17β-hydroxysteroid dehydrogenase type 1 with 3-hydroxyestra-1,3,5,7-tetraen-17-one (equilin) and $NADP^+$, *Proc. Natl. Acad. Sci. U.S.A. 96*, 840−845.
24. Haapalainen, A. M., Koski, M. K., Qin, Y. M., Hiltunen, J. K., and Glumoff, T. (2003) Binary structure of the two-domain (3R)-hydroxyacyl-CoA dehydrogenase from rat peroxisomal multifunctional enzyme type 2 at 2.38 Å resolution, *Structure 11*, 87−97.

25. Haapalainen, A. M., Koski, M. K., Qin, Y. M., Hiltunen, J. K., and Glumoff, T. (2003) Binary structure of the two-domain (3R)-hydroxyacyl-CoA dehydrogenase from rat peroxisomal multifunctional enzyme type 2 at 2.38 Å resolution, *Structure 11*, 87−97.
26. Ghosh, D., Pletnev, V. Z., Zhu, D. W., Wawrzak, Z., Duax, W. L., Pangborn, W., Labrie, F., and Lin, S. X. (1995) Structure of human estrogenic 17β-hydroxysteroid dehydrogenase at 2.20 Å resolution, *Structure 3*, 503−513.
27. Liao, D., Basarab, G. S., Gatenby, A. A., Valent, B., and Jordan, D. B. (2001) Structures of trihydroxynaphthalene reductase-fungicide complexes: Implications for structure-based design and catalysis, *Structure 9*, 19−27.
28. Duax, W. L., Pletnev, V., Addlagatta, A., Bruenn, J., and Weeks, C. M. (2003) Rational proteomics I. Fingerprint identification and cofactor specificity in the short-chain oxidoreductase (SCOR) enzyme family, *Proteins 53*, 931−943.
29. Haapalainen, A. M., Koski, M. K., Qin, Y. M., Hiltunen, J. K., and Glumoff, T. (2003) Binary structure of the two-domain (3R)-hydroxyacyl-CoA dehydrogenase from rat peroxisomal multifunctional enzyme type 2 at 2.38 Å resolution, *Structure 11*, 87−97.
30. Rozwarski, D. A., Vilcheze, C., Sugantino, M., Bittman, R., and Sacchettini, J. C. (1999) Crystal structure of the *Mycobacterium tuberculosis* enoyl-ACP reductase, InhA, in complex with NAD^+ and a C16 fatty acyl substrate, *J. Biol. Chem. 274*, 15582−15589.
31. Lo Conte, L., Chothia, C., and Janin, J. (1999) The atomic structure of protein−protein recognition sites, *J. Mol. Biol. 5*, 2177−2198.
32. Alberts, P., Engblom, L., Edling, N., Forsgren, M., Klingstrom, G., Larsson, C., Ronquist-Nii, Y., Ohman, B., and Abrahmsen, L. (2002) Selective inhibition of 11β-hydroxysteroid dehydrogenase type 1 decreases blood glucose concentrations in hyperglycaemic mice, *Diabetologia 45*, 1528−1532.
33. Walker, B. R., Connacher, A. A., Lindsay, R. M., Webb, D. J., and Edwards, C. R. (1995) Carbenoxolone increases hepatic insulin sensitivity in man: A novel role for 11-oxosteroid reductase in enhancing glucocorticoid receptor activation, *J. Clin. Endocrinol. Metab. 80*, 3155−3159.

BI047599Q